Università di Pisa

DESTEC
Dipartimento di Ingegneria dell'Energia, dei Sistemi, del Territorio e delle Costruzioni

Magnetic levitation sliding systems

Magnetic field evaluation

EMLab
Applied Electromagnetics Laboratory

ironlev

April 14, 2025

Authors

Claudia Simonelli, Nicolò Gori, Antonino Musolino, Luca Sani, Rocco Rizzo

Disclaimer

Contact

Largo Lucio Lazzarino, 1
56122, Pisa
Italy

+39 050 2217302

Contacts: claudia.simonelli@unipi.it, rocco.rizzo@unipi.it

Contents

1 Motivation

This study was carried out to analyze the behavior of the magnetic levitation sliding systems produced by IronBox Srl with respect to the packing instructions for air transport of magnetic materials and the guidelines on limits of exposure to static magnetic fields in conformity with the standard UN 2807, Class 9. According to the International Civil Aviation Organization (ICAO) Technical Instructions (TI) [1], the article is not restricted as a magnetized material (UN 2807, Class 9) if the amplitude of the maximum field observed at a distance of 2.1 m is less than $H_\ell = 0.159$ A/m. This limit, in air, can be expressed in terms of magnetic flux density, as:

$$B_\ell = \mu_0 H_\ell \approx 200\,\mathrm{nT},$$

where $\mu_0 = 4\pi \cdot 10^{-7}\ H/m$ is the vacuum magnetic permeability.

Concerning the limit of exposure to static magnetic fields, the International Commission on Non-Ionizing Radiation Protection (ICNIRP) established it to 400 mT for the general public exposure of any part of the body [2].

The analysis carried out with the methodology described in the following Sections, using the information about the device provided by IronBox Srl, revealed the compliance of the slider with both these limits.

2 Methodology

Given the difficulties to measure very low values of the magnetic flux density, due to the interference of the environment, the uncertainties related to the probe resolution and so on, in this report a hybrid methodology was used. It is based on the development of a numerical model of the device under evaluation, validated with experimental measurements in the near-field region. Then, the magnetic field at larger distances was evaluated by the simulation performed with the numerical model. The numerical analysis is based on 3D-Finite Element (FE) Models obtained by using two different codes (i.e., Simcenter MagNet [3] and EFFE [4]). As for the validation, experimental measurements were performed at different positions using two probes with different ranges. In particular, simulation results at distances of 20 cm and 40 cm were compared with measurements performed with the *AlphaLab DC Milligauss Meter Model MGM*. Instead, simulation values for distances lower than 10 cm were validated by measuring the magnetic field with the *Lakeshore F71 Teslameter* with a three-axis field probe.

In order to measure the magnetic flux density in the near-field region, the device was placed on a moving platform (refer to Figure 1), able to precisely control the position in the space, move along the three axes and rotate about the vertical axis. The amplitude of the magnetic

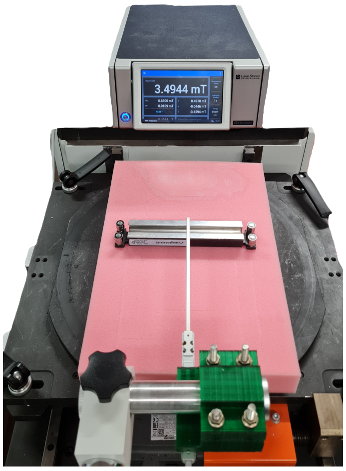

Figure 1: Experimental setup used to measure the magnetic field.

flux density produced by the slider was measured using the *Lakeshore* field probe fixed to a support. The relative position between the slider and the probe was varied in a reduced volume using the moving platform, and the magnetic flux density was measured by changing the slider position. The effect of the iron rail on the magnetic field was also considered by performing the same analysis in both conditions (i.e., without and with the rail in the slider). The *AlphaLab* probe, instead, was used to evaluate the field in the far-field region, reducing the interference with the environment.

3 Slim slider

The device under investigation is shown in Figure 2. The overall dimensions of the slider are 180x31x21.1 mm, while the rail section diameter is 9 mm.

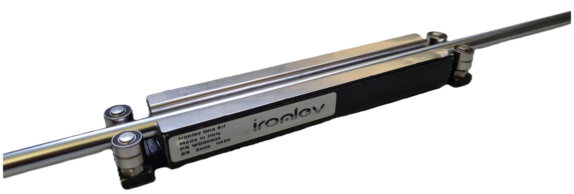

Figure 2: IronBox Slim slider system.

The magnetic field behavior was investigated as a function of the distance from the slider. The following analyses were carried out considering the system of coordinates visible in Figure 3. The Slim slider behavior was analyzed using two different FE software (i.e., Sim-

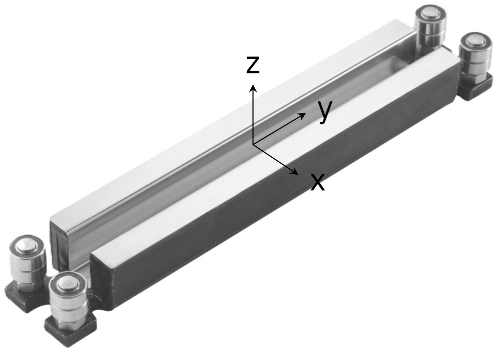

Figure 3: System of coordinates.

center MagNet and EFFE). Their results were validated by comparing them with measurements of magnetic flux density near the slider, as described in the previous Section. The validated models were then used to investigate the magnetic field behavior 2.1 m away from the slider.

Figure 4 reports the FE model used to derive the magnetic field near the slider with *Simcenter MagNet*, together with the solution mesh through which the magnetic flux density distribution in the slider was derived. The 3D FE model, mesh and magnetic flux density

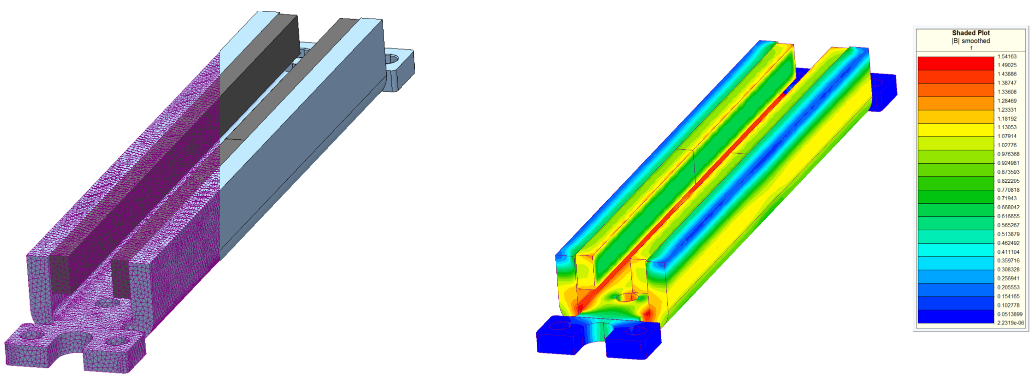

(a) (b)

Figure 4: Full-3D FE model of the Slim slider in Simcenter MagNet width detail of the mesh and magnetic flux density map.

with the EFFE code are shown in figures Figure 5, Figure 6, Figure 7, and Figure 8.
Even if both the FE models show good consistency with respect to experimental data in the near-field region, the reliability of measurements in the far-field one was limited: due to the

small resolution of the far-field probe, that is several times less the amplitude of the Earth field, measurements may be affected by interference. For this reason, the magnetic flux density at large distances from the slider was obtained using the EFFE software.

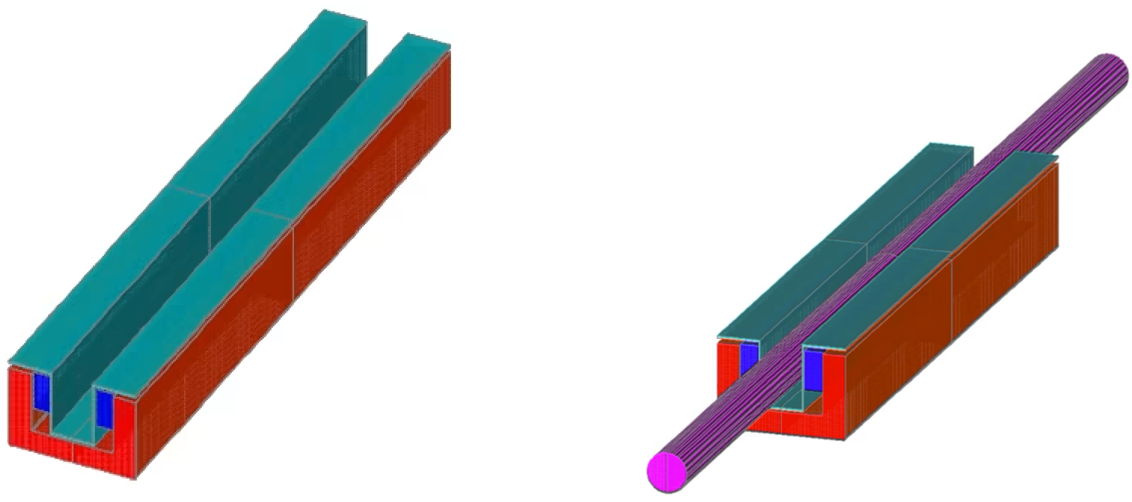

(a) (b)

Figure 5: Full-3D FE models of the Slim slider in EFFE: configurations without (a) and with (b) the iron rail.

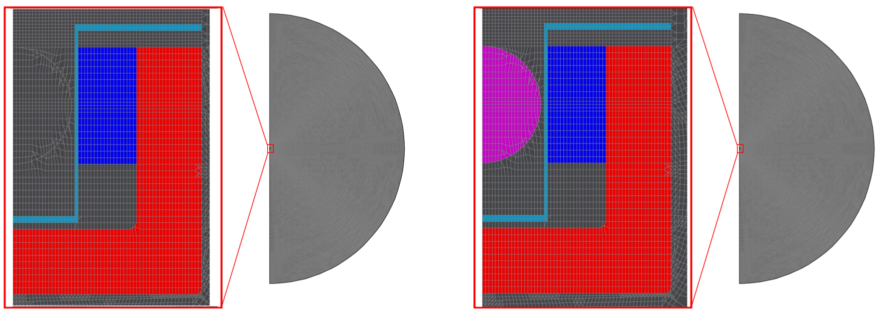

(a) (b)

Figure 6: Details of the mesh of the Slim slider FE models in EFFE: configurations without (a) and with (b) the iron rail.

3.1 Near-field region

The magnetic induction produced by the slider assumes its maximum value near the system. In particular, both without and with the iron rail, the maximum value occurs on the top of the slider, in correspondence with the boundary of the magnet on the opposite part with respect to the ferromagnetic support (ref. Figure 8). The slider compliance with the limits

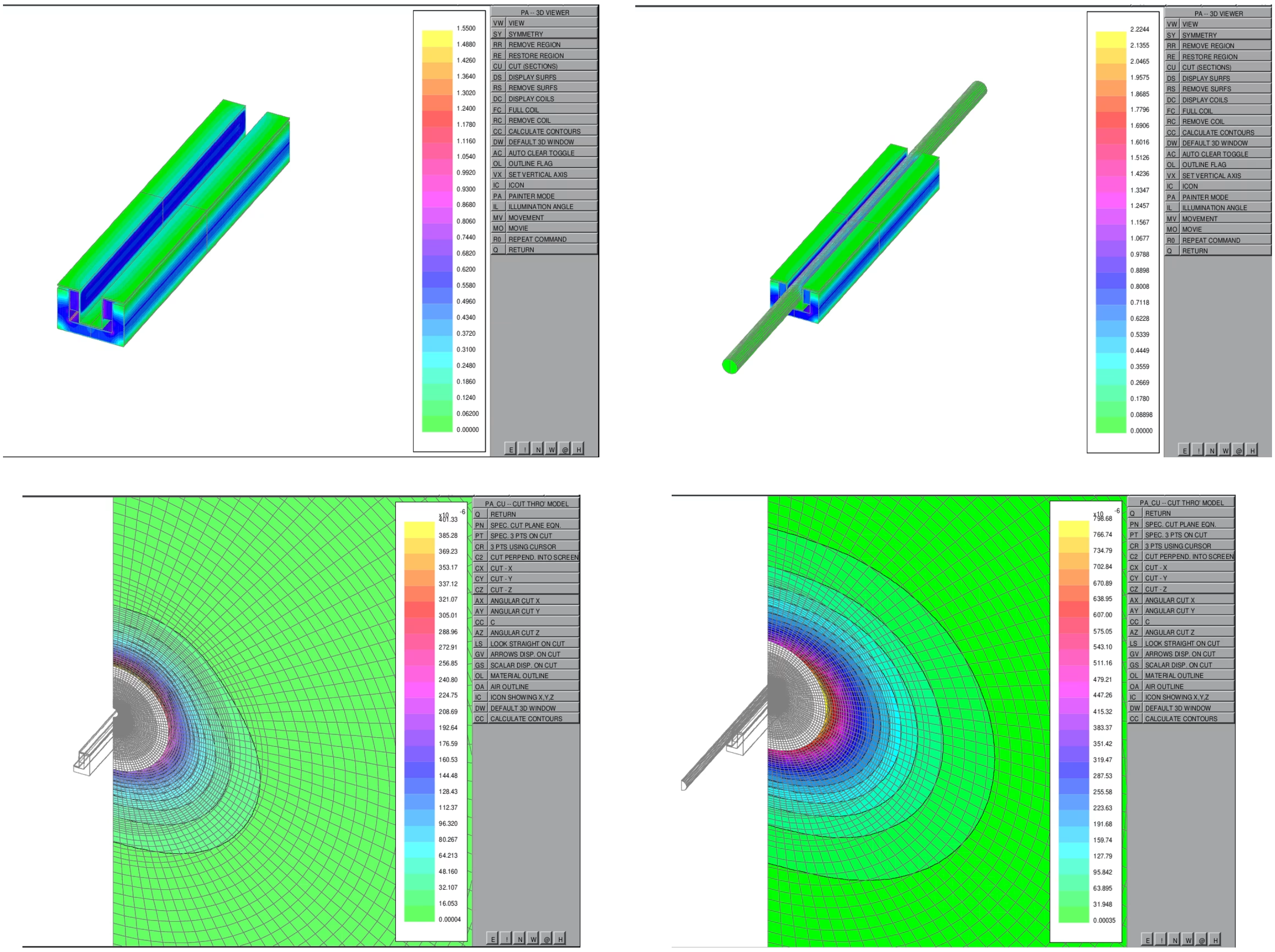

(a) (b)

Figure 7: FE models in EFFE: magnetic flux density maps (without (a) and with (b) the iron rail).

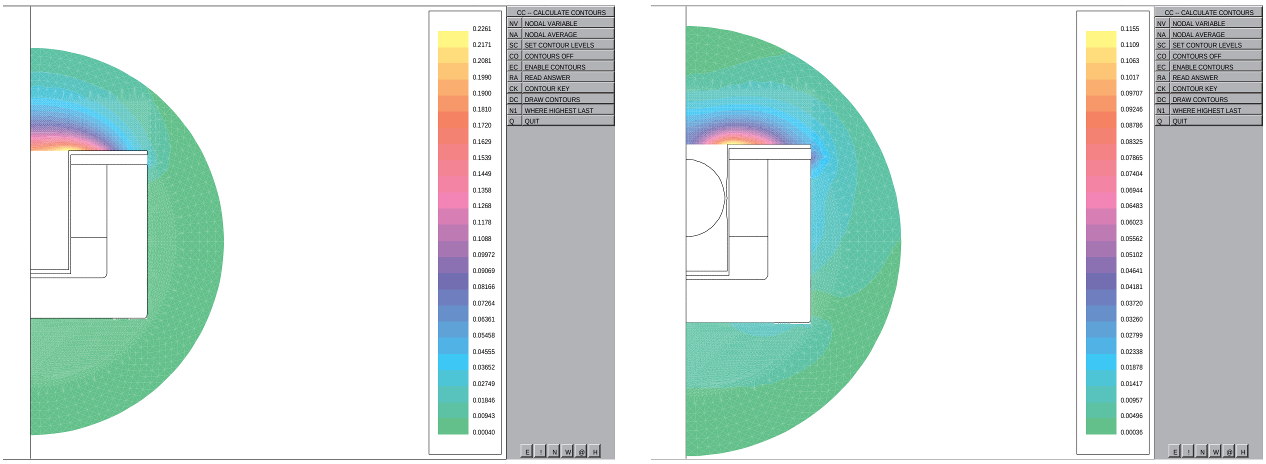

(a) (b)

Figure 8: FE models in EFFE: magnetic flux density maps near the slider (without (a) and with (b) the iron rail).

established by the ICNIRP can be verified by deriving the magnetic flux density amplitude near the system.

Figure 9 reports the behavior of the magnetic induction amplitude with respect to the y-axis direction (see Figure 3), both without and with the iron rail, in correspondence with the point of maximum field on the x-z plane. Simulation results were compared with measures data, highlighting acceptable errors in both conditions, also considering the uncertainties related to the probe position. The maximum value of the magnetic flux density resulted in about 225 mT, obtained without the iron rail.

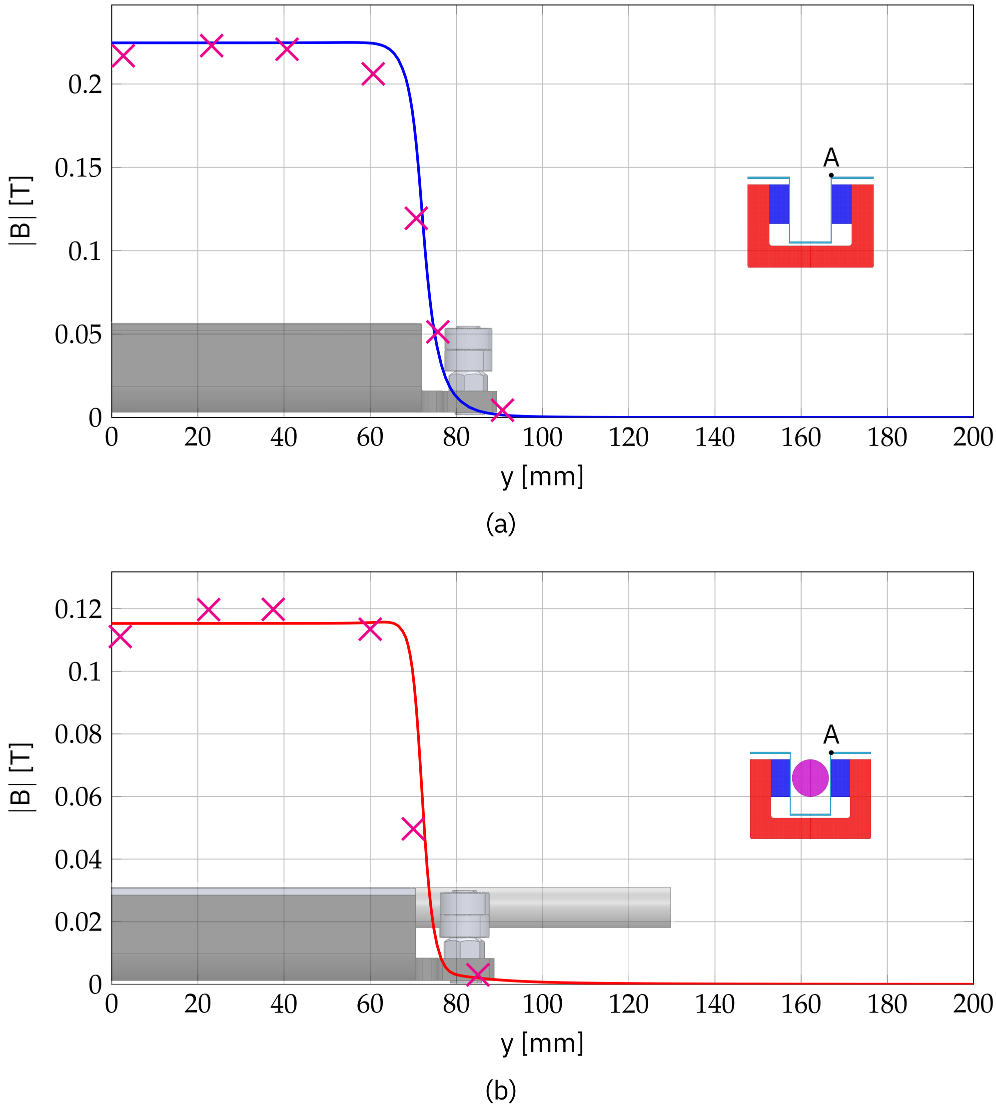

Figure 9: Amplitude of the magnetic flux density as a function of the displacement along the y-axis without (a) and with (b) the iron rail inserted. Values refer to points in correspondence with the top of the slider in the point of maximum field (see point **A**) with y ranging from 0 cm to 20 cm. The magenta crosses highlight experimentally obtained data, with acceptable errors in both conditions, also considering the uncertainties related to the probe position.

The near-field behavior was derived also with respect to the x-axis direction. Figure 10 reports it for x sweeping from 0 mm (i.e., the center of the slider) and 14 mm, in correspondence with the top of the slider and at its center along the y-axis direction (i.e., y=0 referring to the coordinate system in Figure 3). Once again, the behavior was investigated without and with the iron rail, highlighting a smaller field at the same distance when the iron rail was inserted. Simulation results were compared with measured data, resulting in acceptable errors both without and with the iron rail.

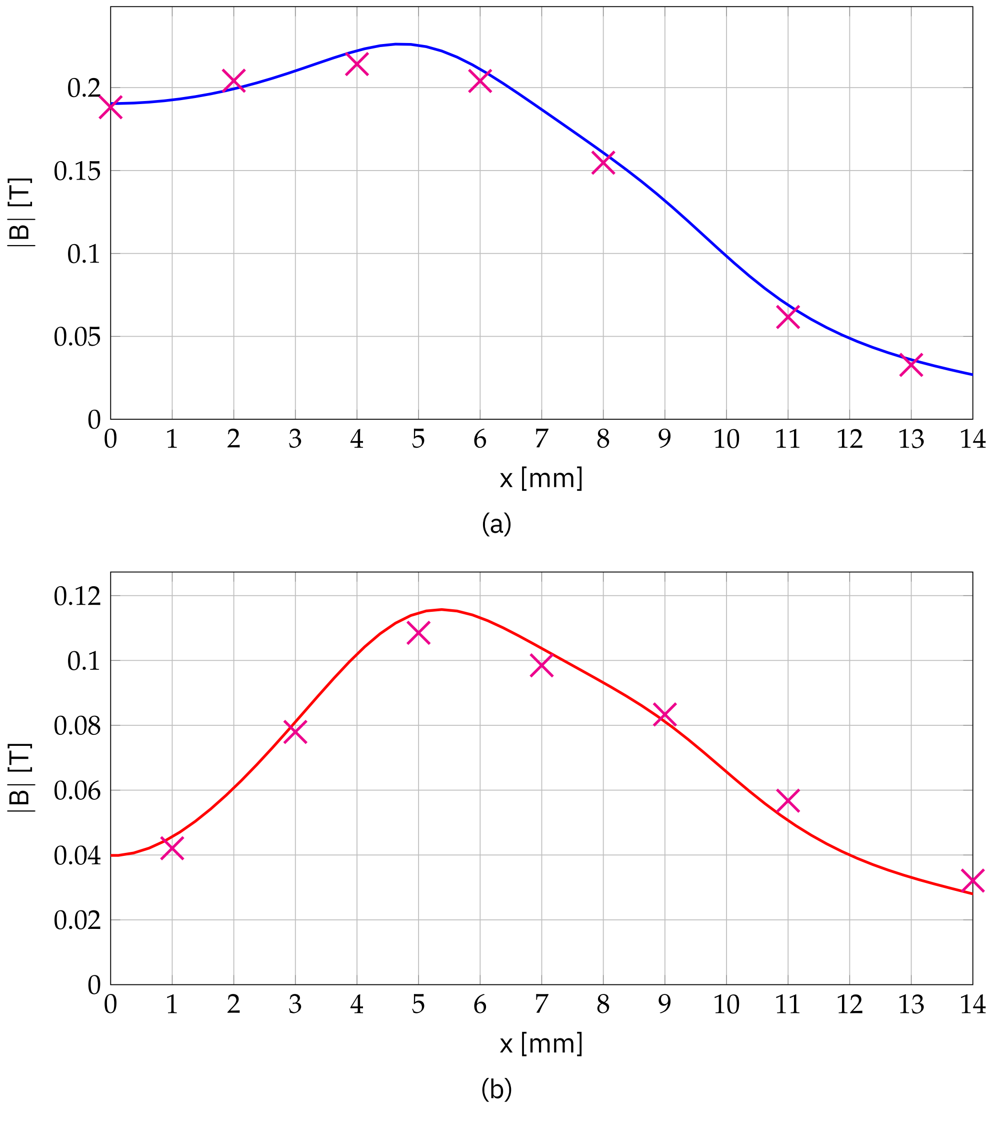

Figure 10: Amplitude of the magnetic flux density as a function of the displacement along the x-axis without (a) and with (b) the iron rail inserted. Values correspond to points in contact with the upper part of the slider with x ranging from 0 cm to 14 mm. The magenta crosses highlight experimentally obtained data.

3.2 Far-field region

The magnetic field behavior far from the slider was investigated to verify the compliance with the ICAO TI guidelines, deriving the amplitude of the magnetic induction produced by the slider at various distances.

3.2.1 Behavior with respect to the x-axis and z-axis directions

Figure 11 reports the simulated behavior of the magnetic flux density amplitude on a circumference with a radius of 5 cm and the center in the middle of the slider. It is worth noticing that the iron rail amplifies the magnetic flux density produced by the slider. This behavior may be accounted for the material saturation, due to the decrease of the reluctance of the magnetic circuit in presence of the rail. Simulation results without and with the iron rail were compared with the measured values, highlighting small errors in both of the cases.

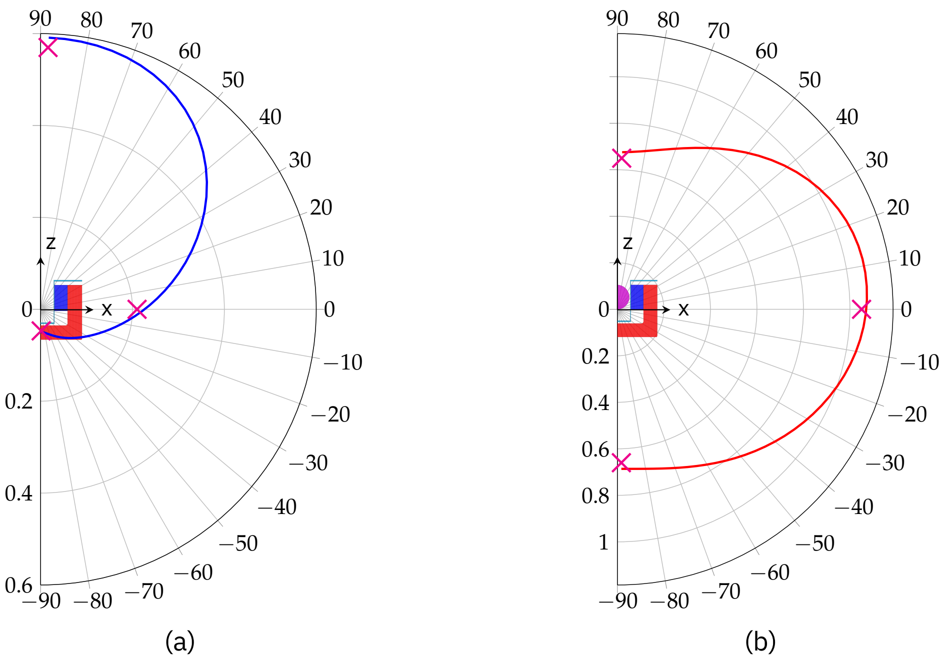

Figure 11: Amplitude of the magnetic flux density at a distance of 5 cm from the center of the slider as a function of the angle position without (a) and with (b) the iron rail. Values are expressed in mT. The magenta crosses highlight experimentally obtained data.

The magnetic flux density amplitude was also derived at higher distances from the slider. Simulation results in terms of magnetic flux density amplitude without and with the iron rail on a circumference with radii of 10 cm, 20 cm, and 40 cm and the center in the middle of the slider are visible in Figure 12, 13, and 14, respectively. Also in these cases, errors between

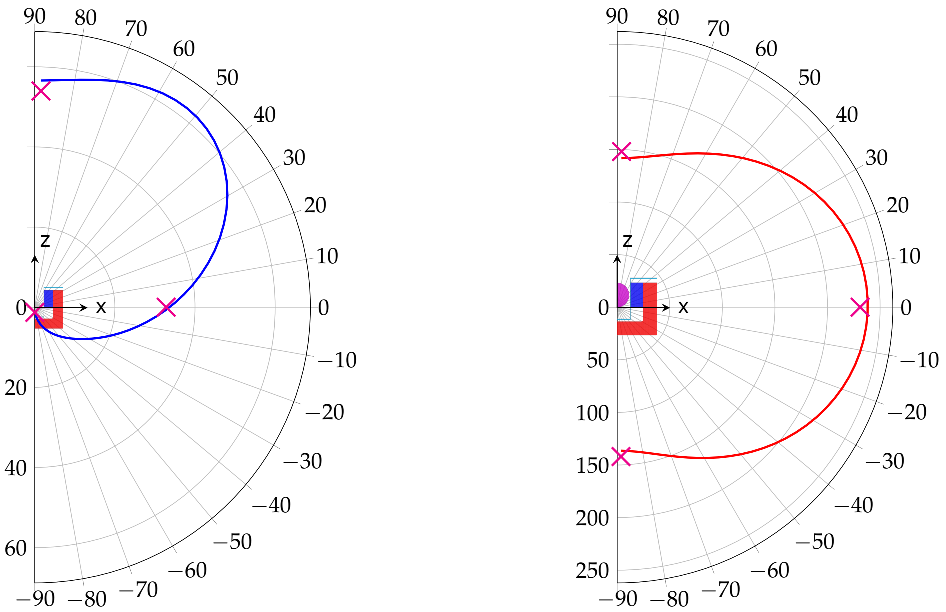

(a) (b)

Figure 12: Amplitude of the magnetic flux density at a distance of 10 cm from the center of the slider as a function of the angle position without (a) and with (b) the iron rail. Values are expressed in μT. The magenta crosses highlight experimentally obtained data.

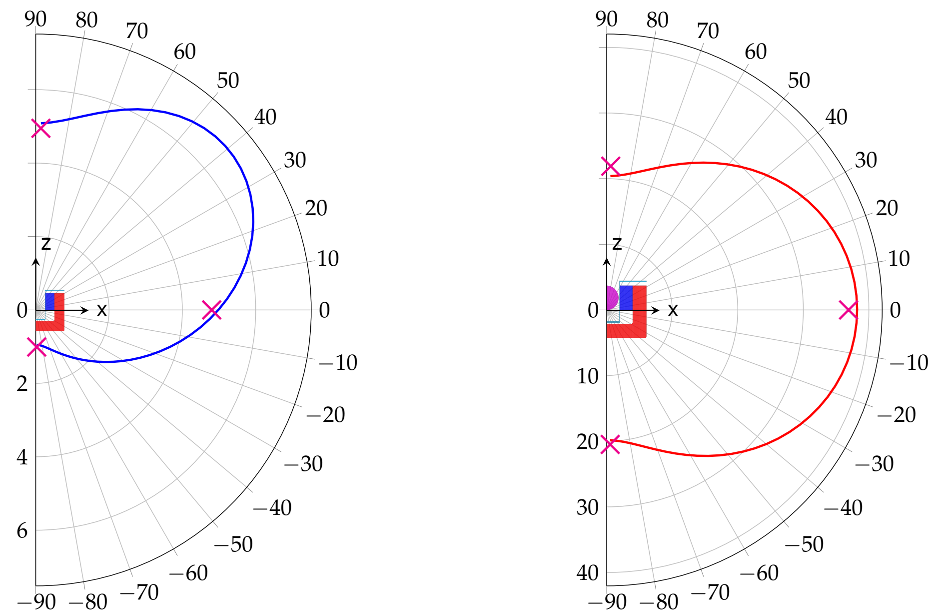

(a) (b)

Figure 13: Amplitude of the magnetic flux density at a distance of 20 cm from the center of the slider as a function of the angle position without (a) and with (b) the iron rail. Values are expressed in μT. The magenta crosses highlight experimentally obtained data.

simulated and measured data were acceptable.

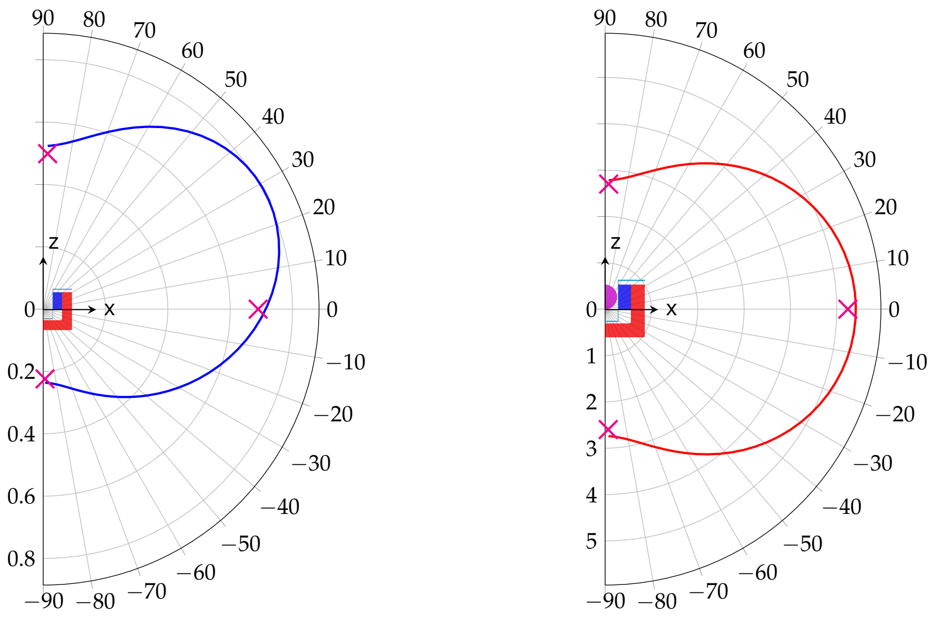

(a) (b)

Figure 14: Amplitude of the magnetic flux density at a distance of 40 cm from the center of the slider as a function of the angle position without (a) and with (b) the iron rail. Values are expressed in μT. The magenta crosses highlight experimentally obtained data.

The same model was used to derive the magnetic flux density amplitude at a distance of 2.1 m from the slider. In particular, Figure 15 reports the amplitude of the magnetic flux density on a circumference with a radius of 2.1 m and the center in the middle of the slider without and with the iron rail. The maximum values of the magnetic induction amplitude resulted in about 4 nT and 30 nT, respectively.

The presence of the iron rail changes the direction of maximum magnetic flux density. Considering the behavior under 5 cm of distance, the magnetic induction is maximum in correspondence with an angle of 90 degrees when the iron rail is not inserted, while it assumes its maximum value for an angle of 0 degrees if the iron rail is present (ref. Figure 11). The behavior along these directions of the magnetic induction amplitude for distances starting from 15 mm to 3 m from the slider are reported in Figure 16.

3.2.2 Behavior with respect to the y-axis direction

The behavior of the magnetic flux density amplitude with respect to the distance along the y-direction (referring to the system of coordinates in Figure 3) was investigated in correspondence with different distances along the x-axis and z-axis directions. The system was

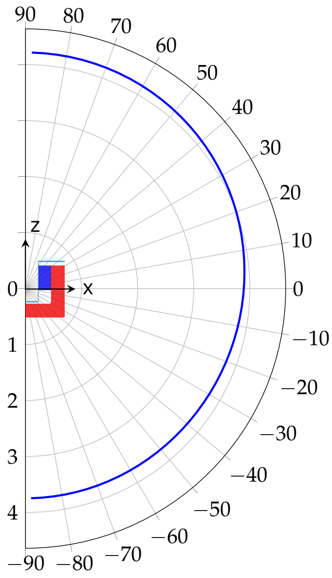

(a)

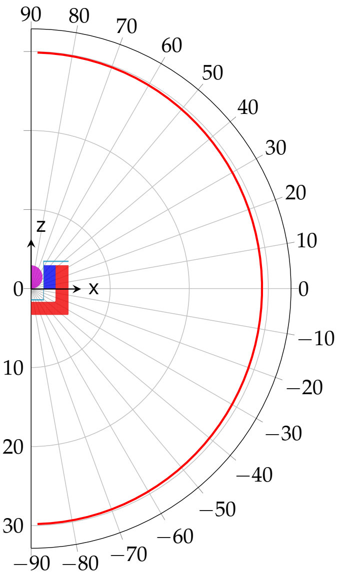

(b)

Figure 15: Amplitude of the magnetic flux density at a distance of 2.1 m from the center of the slider as a function of the angle position without (a) and with (b) the iron rail. Values are expressed in nT.

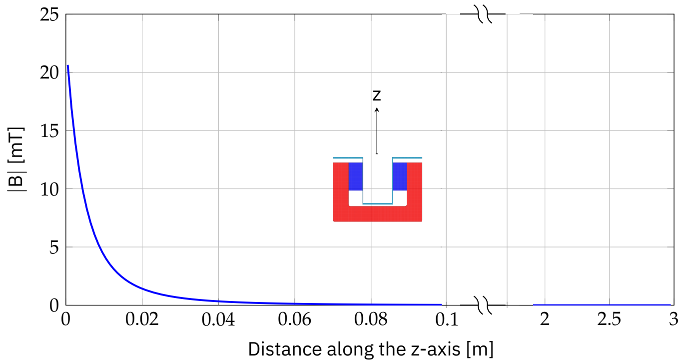

(a)

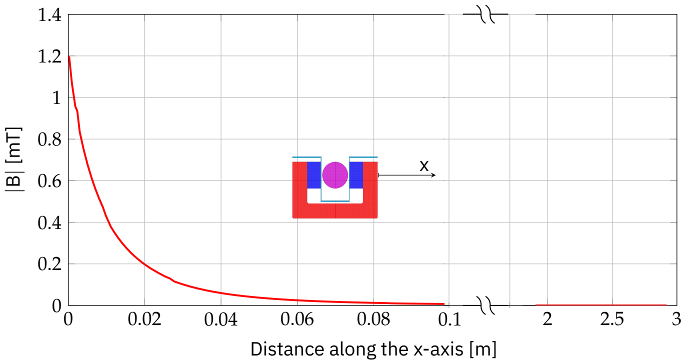

(b)

Figure 16: Amplitude of the magnetic flux density along the z-axis without the iron rail (a) and the x-axis with the iron rail (b). Values correspond to points in the direction of maximum field in both configurations.

first observed at a distance of about 10 cm along the x-direction, at a height corresponding to the center of the slider along the z-direction. The magnetic flux density amplitude at y-direction distances from the middle of the slider in the range [0;3] m are reported in Figure 17. The simulation results for y distances below 15 cm were compared with measured values. The comparison was performed without and with the iron rail, highlighting small errors in both conditions. The simulated values of the magnetic flux density amplitude at a distance of 2.1 m resulted in about 4 nT without the iron rail and 30 nT with the iron rail inserted in the slider. Both values are below the reference one set by the ICAO TI. These values decreases to about 1.5 nT and 11 nT, respectively if distance from the slicer along the x-axis direction become 2.1 m (ref. Figure 18).

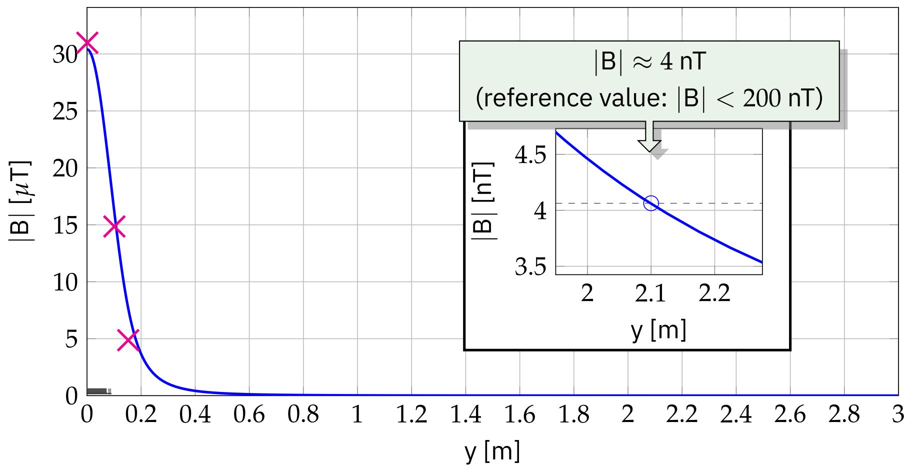

(a)

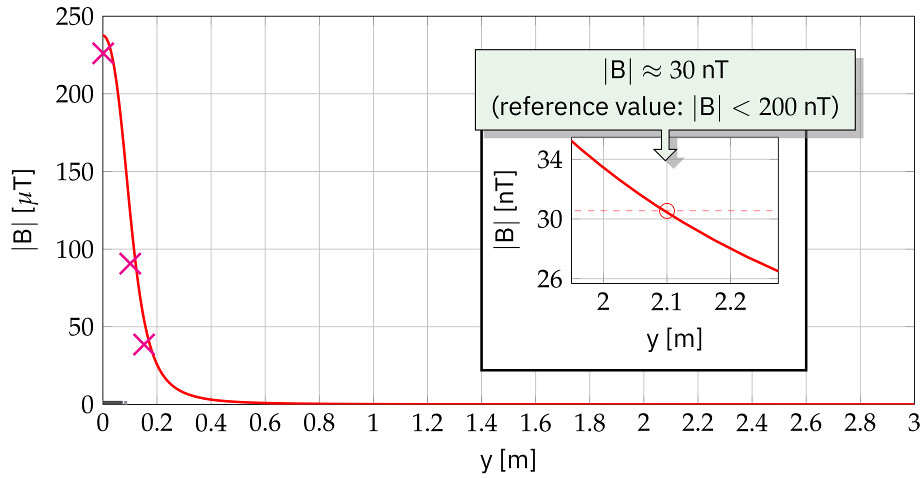

(b)

Figure 17: Amplitude of the magnetic flux density as a function of the displacement along the y-axis without (a) and with (b) the iron rail inserted. Values correspond to points at a height corresponding to the center of the slider along the z-direction, and a position of 10 cm in the x-axis direction. The magenta crosses highlight experimentally obtained data, with small errors in both conditions.

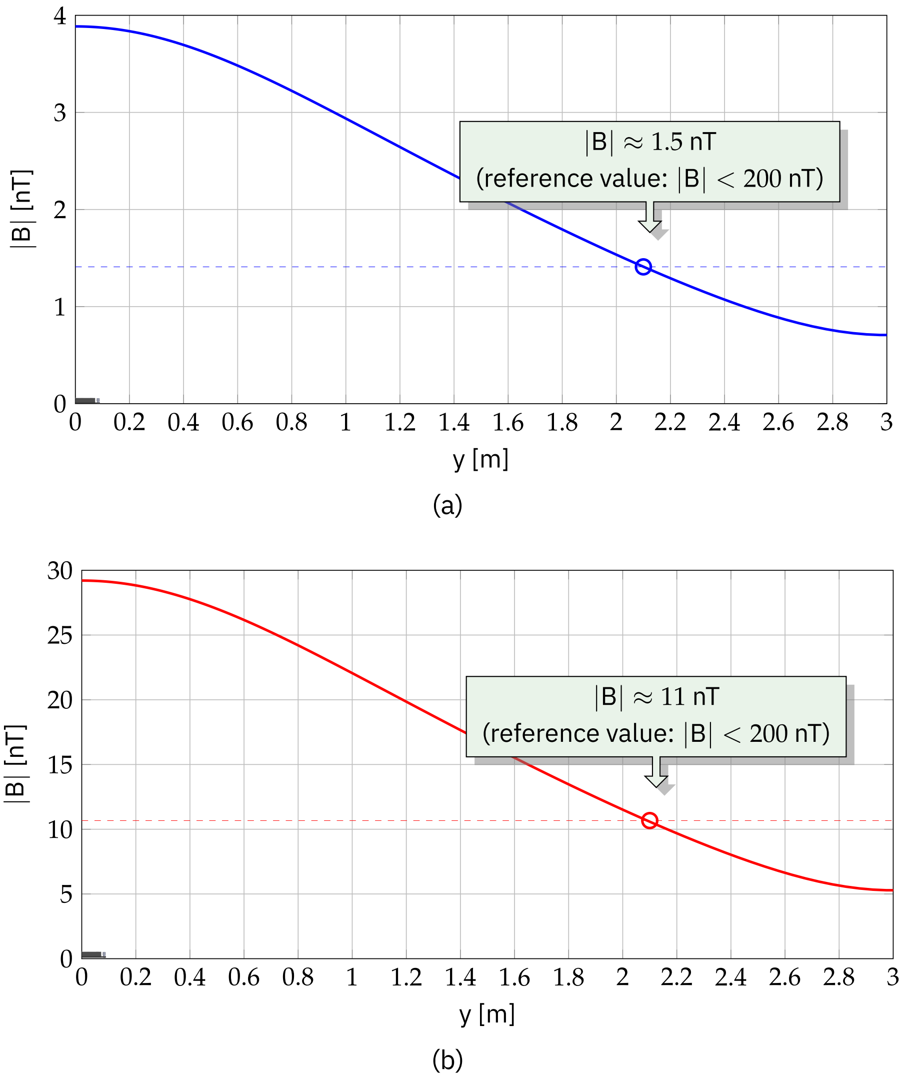

Figure 18: Amplitude of the magnetic flux density as a function of the displacement along the y-axis without (a) and with (b) the iron rail inserted. Values correspond to points at a height corresponding to the center of the slider along the z-direction, and a position of 2.1 m in the x-axis direction.

4 Conclusions

This preliminary study aimed to analyze the behavior of the analyzed magnetic slider with respect to the air transport regulation of magnetic materials and the guidelines on limits of exposure to static magnetic fields. According to the ICAO guidelines, the article is not restricted as a magnetized material if the amplitude of the maximum field observed at a distance of 2.1 m is less than 0.159 A/m (i.e., the maximum magnetic flux density is less than 200 nT). As for the exposure to static magnetic fields, the ICNIRP directives set the limit to 400 mT.

A hybrid methodology was used to investigate the magnetic flux density produced by the

IronBox Slim slider device, without or with the iron rail. Measured data were used to verify the consistency of FE models, which were then used to analyze the magnetic flux density behavior until a distance of 2.1 m.

According to our analysis, carried out with the methodology described, the investigation shows that the slider produces a magnetic flux density of less than about 4 nT at a distance of 2.1 m when the iron rail is not inserted. This value grows to about 30 nT if the iron rail is present. In both configurations, the magnetic flux density at 2.1 m is lower than the limit of 200 nT.

Concerning the near-field results, simulated and measured data highlighted a maximum value of magnetic flux density of about 225 mT without the iron rail and about 115 mT with the iron rail inserted. Both values are smaller than the limit of 400 mT.

However, further in-depth analyses may be performed in order to confirm these results by means other models (e.g., [5, 6, 7, 8]).

References

[1] *DGP-WG/03-WP/51 14/2/03*. URL: `https://www.icao.int/safety/DangerousGoods/WG03/DGPWP03.051.PDF`.

[2] *Linee guida sui limiti di esposizione a campi magnetici statici*. URL: `https://www.icnirp.org/cms/upload/publications/ICNIRPFactSheetStaticFieldsItalian.pdf`.

[3] *Simcenter MagNet, Manual*.

[4] *EFFE v3.04 user manual, Bathwick Electrical Design ltd*. 2024.

[5] W. L. Eichhorn. “Magnetic dipole moment determination by near-field analysis”. In: *NASA Goddard Space Flight Center, Greenbelt, MD, USA* Tech. Rep. TN D-6685 (1972).

[6] K. Liu, Y. Sui, H. Cheng, Z. Wang, and D. A. Clark. “Magnetic Dipole Moment Determination Using Near-Field Magnetic Gradient Tensor Data”. In: *IEEE Geoscience and Remote Sensing Letters* 18.7 (2021), pp. 1169–1173.

[7] T. Nara, S. Suzuki, and S. Ando. “A Closed-Form Formula for Magnetic Dipole Localization by Measurement of Its Magnetic Field and Spatial Gradients”. In: *IEEE Transactions on Magnetics* 42.10 (2006), pp. 3291–3293.

[8] K. Seleznyova, M. Strugatsky, and J. Kliava. “Modelling the magnetic dipole”. In: *European Journal of Physics* 37.2 (Feb. 2016), p. 025203.